Supplementary Material; A field induced modulated state in the ferromagnet PrPtAl

Christopher D. O'Neill,[1] Gino Abdul-Jabbar,[1] Didier Wermeille,[2]
Philippe Bourges,[3] Frank Krüger,[4,5] and Andrew D. Huxley[1]

[1]*School of Physics and CSEC, University of Edinburgh, Edinburgh, EH9 3JZ, UK.*
[2]*XMAS, ESRF, BP220, F-38043 Grenoble, France.*
[3]*Laboratoire Léon Brillouin (UMR12 CEA-CNRS), 91191 Gif-sur-Yvette Cedex, France*
[4]*London Centre for Nanotechnology, University College London,*
Gordon St., London, WC1H 0AH, United Kingdom
[5]*ISIS Facility, Rutherford Appleton Laboratory, Chilton,*
Didcot, Oxfordshire OX11 0QX, United Kingdom
(Dated: December 7, 2020)

I. CRYSTAL GROWTH

High-quality single crystals (RRR ≈ 75) were grown from stoichiometric masses of starting materials under ultra high vacuum by Czochralski pulling from a RF-heated melt in a water cooled crucible. Before the growth Pr (99.9% Ames) and Pt (99.995% Alfa Aesar) were outgassed by ultra high vacuum annealing (Pr and Al (99.999%) were also etched to remove surface oxide).

II. RESONANT X-RAY SCATTERING

Resonant X-ray diffraction was carried out at the XMAS UK-CRG beamline (BM28), ESRF. The sample (crystal mosaic FWHM 0.01°) had a natural as grown surface perpendicular to the c-axis. Measurements were carried out at the 6.444 keV Pr L_2 edge, where a sharp maximum in absorption, fluorescence and magnetic scattering occurs. This comes from a simple dipole transition, confirmed from an azimuthal scan in zero field (for $q_2 = (0, 0, 2.07)$ at 5K) [1]. Fields of up to 4 T were applied with a superconducting magnet (horizontal field transverse to the incident beam), with a 180° vertical and ±5° horizontal aperture. The orientation of the sample cryostat can be set independently of the magnet, and was aligned with the magnet dismounted to give a wider angular coverage, setting the sample b-axis parallel to the magnet table with a precision comparable to the sample mosaic. Measurements were made in the vertical scattering plane, with a LiF (220) analyser to detect scattering in the $\sigma\pi$ channel (Fig. 1, main text). This geometry is sensitive to moments in the ac plane. The error in aligning the b-axis with the field is then the larger of 0.01° and the precision with which the field is parallel to the magnet axis, estimated to be better than 0.1°.

Measurements with field parallel to the a-axis (Fig. 2, main text) were made with the same scattering geometry (ac scattering plane) but the field was applied with a small electromagnet along the a-axis and rotated with the sample (the field was determined with a Hall probe). This set-up had a reduced air gap and hence reduced attenuation from air.

Measured satellite intensities have been normalised to the (002) structural Bragg reflection, to allow comparison of intensities between different setups. At the (002) position, the component of the moment canted along the c-axis has a zero structure factor. Thus for both field orientations the measurements made close to this position are primarily sensitive to the modulated moment along the a-axis.

III. INELASTIC NEUTRON SCATTERING

Inelastic neutron scattering was carried out with the 4F2 cold neutron triple-axis spectrometer at the LLB with a system of double pyrolytic graphite monochromators and a pyrolytic graphite analyzer. A beryllium filter was put on the final energy arm to remove higher order reflections. The analyzer was kept flat throughout the experiment, with no horizontal or vertical focusing. No collimator was used. The experiment was carried out with fixed final neutron energy of $k_f = 1.3$ Å^{-1}. The single crystal sample was mounted with [H0L] in the scattering plane and fields of up to 7 T were applied along the b-axis with a superconducting magnet. The sample was mounted on a small goniometer stage and was accurately aligned to have its b-axis vertical, parallel with the field. The diffraction data presented below and the inelastic measurements shown in the main text were measured with the same set-up and experimental

conditions.

Fig. S1 shows the low temperature field dependence of elastic magnetic intensity at the (002) Bragg peak. The nuclear contribution to the scattering was measured in zero field just above T_N and subtracted from the total intensity to give the magnetic intensity. The magnetic intensity is proportional to the total uniform moment squared $M^2 = M_a^2 + M_b^2$, expressed in units μ_B^2 by normalising to the nuclear intensity, assuming a free ion Pr^{3+} form factor. Note that the induced moment along the b-axis is not fully saturated in fields as high as 25 T [2]. The scattering intensity of the SDW3 peak at $q \approx (0, 0, 2.24)$ is also shown in the same intensity units (including a factor of two to account for multiplicity). The data clearly shows that the uniform moment is suppressed (due to a reduction of M_a) when the SDW3 state is formed in increasing field.

IV. RESISTIVITY

Resistivity and magnetoresistance (MR) measurements were made with a standard 4 probe technique (100 μA current applied along the c-axis at 37 Hz). Experiments were carried out in a ^{4}He closed cycle refrigerator with 9 T superconducting magnet. The sample was mounted on a 2-axis rotating stage, fitted with Hall probes to allow accurate adjustment of the applied field direction, to align the field precisely along the b-axis (Fig. 3, main text).

The resistivity at zero field, normalised to the value at 300 K, is shown in Fig. S2(a). This shows a stronger T dependence in the SDW2 state than below or above it, which provides evidence for an enhanced DOS. The MR, normalised to the zero field resistivity value at 300 K, for field along the easy a-axis is shown in Fig. S2(b). The low field MR is strongly negative in the SDW2 state with a cusp-like maximum at $H = 0$, suggesting stronger fluctuations are present in the SDW2 state than in the FM state, supporting a QOBD based explanation for SDW2. The MR for SDW1 has an initial peak at low field, that in the current work we show, is a result of the amplitude of the SDW1 state being initially enhanced with magnetic field. The structure in resistivity, linked to SDW1 and SDW2, is washed out by field along the easy a-axis and is completely absent for B$>$ 40 mT, consistent with the suppression of these states.

V. QUANTUM ORDER BY DISORDER IN THE PRESENCE OF MAGNETIC ANISOTROPY AND FIELD

We analyze if the fermionic quantum order-by-disorder mechanism, in the presence of magnetic anisotropy and magnetic field, can qualitatively explain the experimentally observed phase diagram. For simplicity, we consider electronic quasiparticles with an isotropic dispersion $\epsilon(\mathbf{k}) = \hbar^2\mathbf{k}^2/(2m^*)$ and subject to a local repulsion U. At the mean-field level, the system undergoes a Stoner transition to a ferromagnetic state at $\rho U_c = 1$, where ρ denotes the density of states at the Fermi level. In dimensionless units, the mean-field free energy density is given by $f_{\rm mf} = \alpha(T)\mathbf{m}^2 + \beta\mathbf{m}^4 + \gamma\mathbf{m}^6$, with coefficients $\alpha(T) = 1/(\rho U) - 1 + \frac{\pi^2}{12}(T/T_F)^2$, $\beta = 1/48$ and $\gamma = 1/384$.

The coupling to soft electronic particle-hole fluctuations gives rise to a free energy contribution $\delta f_{\rm fl} = \frac{1}{2}(\lambda\rho U)^2\mathbf{m}^4 \ln[\mathbf{m}^2 + (T/T_F)^2]$ [3], with a dimensionless constants λ. This term renders the Stoner transition unstable to fluctuation-induced first-order behavior below a tricritical point P_c at temperature $T_c = T_F \exp[-\beta/(\lambda\rho U)^2]$. In the following, we will only include the fluctuation contribution $\delta\beta_{\rm fl}(T) = (\lambda\rho U)^2 \ln(T/T_F)$ to the $\mathbf{m}^4$ coefficient. This is sufficient if we want to understand the behaviour near P_c.

It was pointed out in Ref. [4], that Landau damping of the order parameter field gives rise to a negative, non-analytic contribution to the static magnetic susceptibility, rendering the Hertz-Millis-Moriya theory [5, 6] unstable towards first-order behavior and incommensurate order. Such modulated magnetism, is expected, since the resulting deformations of the Fermi surface enhance the phase space for electronic particle-hole fluctuations, a mechanism termed fermionic quantum order-by disorder [7].

Starting from the isotropic electronic model, it is possible to self-consistently calculate fluctuations around a helimagnetic state with ordering wavevector $\mathbf{q}$. The resulting gradient terms in the free energy, are proportional to the coefficients of the $\mathbf{q} = 0$ terms [8, 9],

$$f \;=\; \frac{1}{V}\int \mathrm{d}^3\mathbf{r}\Big\{\alpha\mathbf{m}^2 + (\beta + \delta\beta_{\rm fl})\mathbf{m}^4 + \gamma\mathbf{m}^6 + \frac{2}{3}(\beta + \delta\beta_{\rm fl})(\nabla\mathbf{m})^2 + \gamma\mathbf{m}^2(\nabla\mathbf{m})^2 + \frac{3}{5}\gamma(\nabla^2\mathbf{m})^2\Big\}. \qquad (1)$$

The simultaneous sign change of the $\mathbf{m}^4$ and $(\nabla\mathbf{m})^2$ coefficients demonstrates that the fluctuation-driven first order transition is pre-empted by the formation of a helimagnetic state.

In PrPtAl magnetic anisotropy arises from the coupling of the conduction electrons to local moments. As a result of the c-axis being the hard direction, the ordering wavevector of the modulated states is along the c-direction and the magnetization confined to the a-b plane. In addition, the system exhibits a small in-plane anisotropy,

$$f_{\rm ani} = -\frac{\eta}{V}\int \mathrm{d}^3\mathbf{r}\ (m_a^2 - m_b^2), \tag{2}$$

with $\eta > 0$. Such anisotropy, leads to a deformation of the magnetic helix, resulting in a pronounced third harmonic in the magnetic structure factor. Moreover, since the anisotropy favours the homogeneous ferromagnet over the helimagnet, the region of modulated magnetism is reduced and the transition between the two magnetic phases becomes weakly first order. A representative phase diagram for $\lambda = 0.1$ and small anisotropy $\eta = 10^{-5}$ (in units of ρU^2) is shown in the inset of Fig. S3 as a function of the inverse dimensionless interaction strength $1/(\rho U)$ and dimensionless temperature T/T_F.

We now investigate the effects of a magnetic field along the hard in-plane direction $\mathbf{b}$,

$$f_h = -\frac{h}{V}\int \mathrm{d}^3\mathbf{r}\ m_b. \tag{3}$$

We expect that the helimagnet is stable for small h and described by the order parameter

$$\mathbf{m}_{\rm helix}(\mathbf{r}) = \begin{pmatrix} m_a \cos[qz + \phi(z)] \\ m_b \sin[qz + \phi(z) + \epsilon] \end{pmatrix} \tag{4}$$

with $\phi(z) = -\delta_{1a}\sin(qz) + \delta_{1b}\cos(qz) - \delta_2 \sin(2qz)$. Such a deformed helix with $\delta_1, \delta_2 > 0$ is shown in Fig. S3. The distortion δ_1 tilts the moments towards the field direction (positive b-axis), while δ_2 lowers the anisotropy energy by bunching the moments towards the $\pm a$-axis. Numerical minimization of the free energy shows that higher harmonics of $\phi(z)$ are negligible. We neglect modulations of the amplitude $|\mathbf{m}(\mathbf{r})|$ which are expected to be small.

For larger fields, one might expect that a fan state around the field direction becomes energetically favourable. We therefore consider fan states of the form

$$\mathbf{m}_{\rm fan}(\mathbf{r}) = \begin{pmatrix} m_a \cos\Omega(z) \\ m_b \sin\Omega(z) \end{pmatrix} \tag{5}$$

with $\Omega(z) = \Omega_0 + \Delta\sin(qz)$. Here, Δ is the opening angle of the fan which is centered around the angle Ω_0. Fan states along the field direction are described by $\Omega_0 = \pi/2$, fan states around the easy a axis by $\Omega_0 \in \{0, \pi\}$.

Evaluating the free energy density $f + f_{\rm ani} + f_h$ for the homogeneous ferromagnet, deformed helix and fan states we obtain

$$f_{\rm FM}(m_a, m_b) = \alpha(m_a^2 + m_b^2) + \tilde{\beta}(m_a^2 + m_b^2)^2 + \gamma(m_a^2 + m_b^2)^3 - \eta(m_a^2 - m_b^2) - h\, m_b \tag{6}$$

$$\begin{aligned} f_{\rm helix}(m, q, \delta_1, \delta_2) = {} & \alpha m^2 + \tilde{\beta} m^4 + \gamma m^6 + \frac{2}{3}\tilde{\beta} q^2 m^2 + \frac{3}{5}\gamma q^4 m^2 + \gamma q^2 m^4 + \frac{3}{10}\gamma q^4 m^2(\delta_1^2 + 4\delta_2^2) \\ & - \eta\, m^2\left[J_1(2\delta_2) - J_2(2\delta_1) - \delta_1^2\delta_2\right] - h\, m\left[J_1(\delta_1) + \frac{1}{4}\delta_1\delta_2 - \frac{1}{8}\delta_1\delta_2^2\right] \end{aligned} \tag{7}$$

$$\begin{aligned} f_{\rm fan}(m, q, \Omega_0, \Delta) = {} & \alpha m^2 + \tilde{\beta} m^4 + \gamma m^6 + \frac{1}{3}\tilde{\beta}\Delta^2 q^2 m^2 + \frac{3}{10}\gamma\Delta^2\left(1 + \frac{3}{4}\Delta^2\right) q^4 m^2 + \frac{1}{2}\gamma\Delta^2 q^2 m^4 \\ & - \eta\, m^2 \cos(2\Omega_0) J_0(2\Delta) - h\, m \sin(\Omega_0) J_0(\Delta) \end{aligned} \tag{8}$$

where J_0, J_1 and J_2 denote Bessel functions of the first kind and $\tilde{\beta} = \beta + \delta\beta_{\rm fl}$.

We minimize the free energies for the different states and identify phase transitions from free energy crossings. Since the free energy expansions are only controlled in the close vicinity of P_c, where the magnetization m and the ordering wavevector q are small, it is not possible to map out the full phase diagram. Instead, we fix $1/(\rho U) = 0.997$ and investigate the behavior along different cuts through the h-T phase diagram close to P_c.

In Fig. S3, the free energies of the different modulated states relative to the ferromagnet, $f_{\rm mod} - f_{\rm FM}$, are shown as a function of field, h/η, for a fixed $T/T_F = 0.074$. As shown in the inset, at $h = 0$ this corresponds to a point in the helimagnetic phase above the ferromagnetic region. In the regime of small fields, the deformed helix and the fan states are favored over the homogeneous ferromagnet, where the deformed helix has the lowest free energy. At very small fields, the fan state around the easy axis ($\pm a$ direction) is energetically favored over the fan around the field direction (b axis). The free energies of the two fan states cross at around $h/\eta \approx 1.4$, where the energy scales associated with

the in-plane anisotropy and the applied magnetic field are comparable. At a larger field value of $h/\eta \approx 5.6$, the free energies of the helix and the fan around the field direction cross, indicative of a first-order transition between the two modulated states. The fan remains the state with the lowest free energy up to a field $h/\eta \approx 10.5$ at which the system becomes fully polarized along the field direction. The free energy of the fan state smoothly approaches that of the polarized ferromagnet, suggesting that the transition is continuous.

The nature of the phase transitions is evident from the behavior of the order parameters, shown in Fig. S4. The ordering wavevector q jumps at the first-order transition between the deformed helix and the fan. q has a larger value in the fan state, as seen in experiment. The opening angle Δ of the fan state has a strong field dependence and goes to zero at the continuous transition to the polarized ferromagnet. As expected, the deformation δ_1 of the helix increases linearly with field, while the distortion δ_2 towards the easy axis is determined by the anisotropy η and is almost independent of the applied field. Experimentally δ_1 is smaller than δ_2 over the full field range. This would result from a higher value of η than used in the illustrative calculation. Increasing η increases δ_2 and this in turn reduces the rate of increase of δ_1 with field.

We now investigate the temperature dependence at fixed field $h/\eta = 0.95$, well below the critical field where the first-order transition to the fan state occurs. At such small fields the ferromagnet is stable at low temperatures. The free energy difference $f_{\text{helix}} - f_{\text{FM}}$ (Fig. S5(a)) shows a first-order transition from the ferromagnet to the deformed helix at $T/T_F \approx 0.0688$. As shown in Fig. S5(b), q jumps from zero to a finite value at the transition and increases with temperature.

As in the zero-field case, we don't see any indication for the presence of two modulated states, SDW1 and SDW2, with a jump in q at the transition between the two modulated states. This could be be due to the simplicity of our model which neglects lattice effects, does not correctly account for the electronic bandstructure of PrPtAl, and incorporates local moments only as source of anisotropy.

Nevertheless, the temperature dependence of the deformations δ_1 and δ_2 (Fig. S5(c)) reflects some of the experimentally observed behavior. At low temperatures, δ_2 dominates, giving rise to a strong third harmonic in the magnetic structure factor. As temperature is increased, δ_2 decreases faster than δ_1. Close to the transition to the paramagnet, δ_1 dominates, giving rise to a pronounced second harmonic.

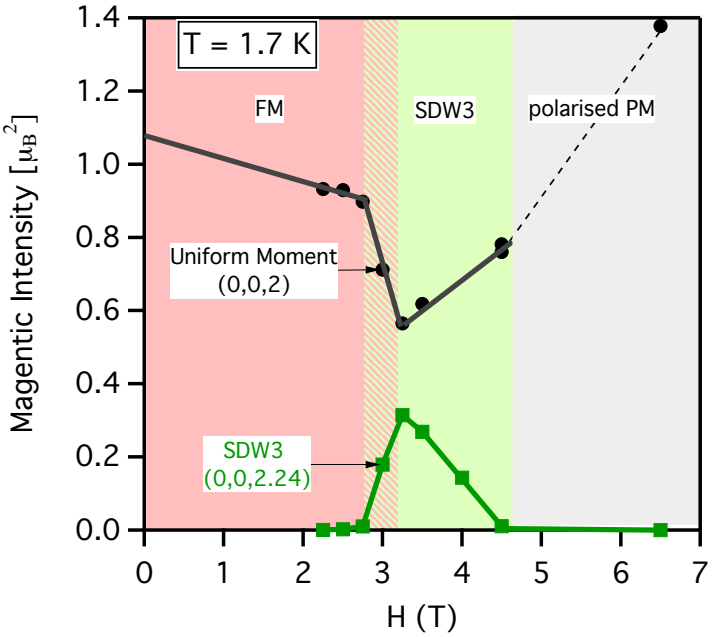

FIG. S1: The low temperature elastic magnetic intensity of the (002) and SDW3 $q \approx (0, 0, 2.24)$ Bragg peaks measured with neutron scattering, as a function of field (H), applied along the b-axis.

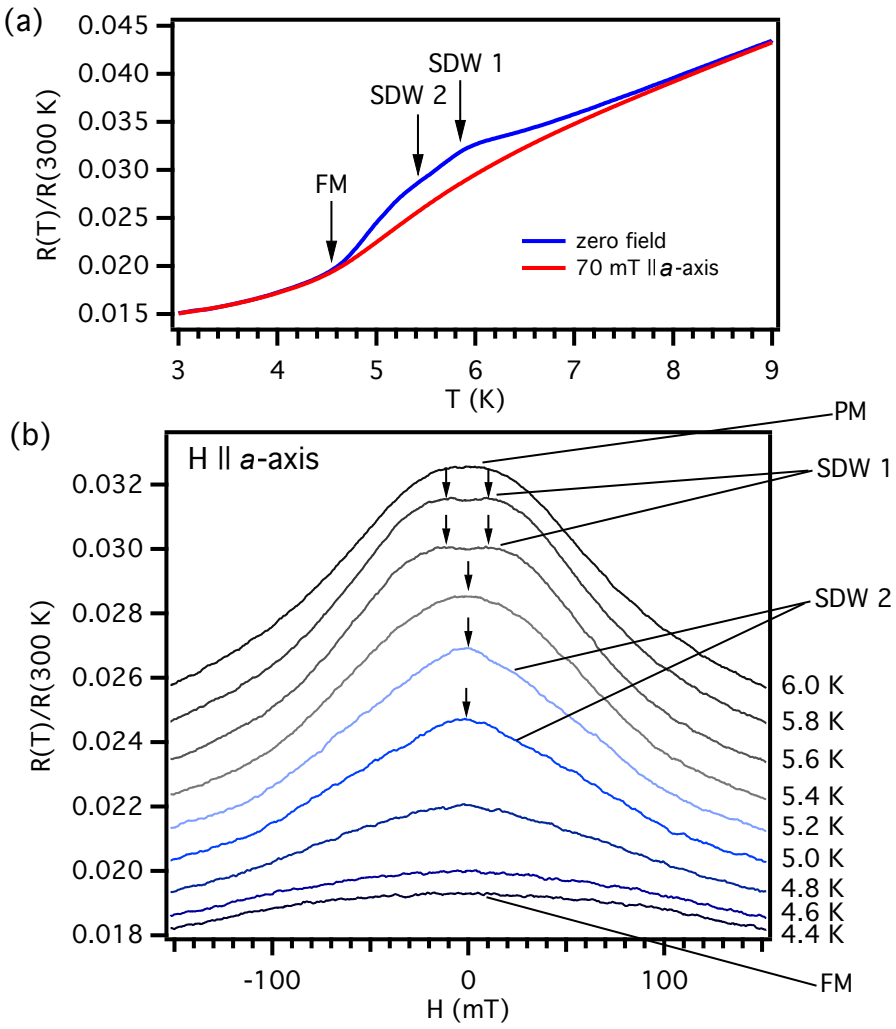

FIG. S2: (a) Low temperature resistivity of PrPtAl normalised to the value at 300 K, at zero field (blue) and 70 mT applied along the a-axis (red). (b) Magnetoresistance for field applied along the a-axis. Arrows indicate the maxima at $\approx$ 10 mT in SDW1 and the cusp in SDW2. Paramagnetic (PM) and ferromagnetic (FM) states are also marked for comparison.

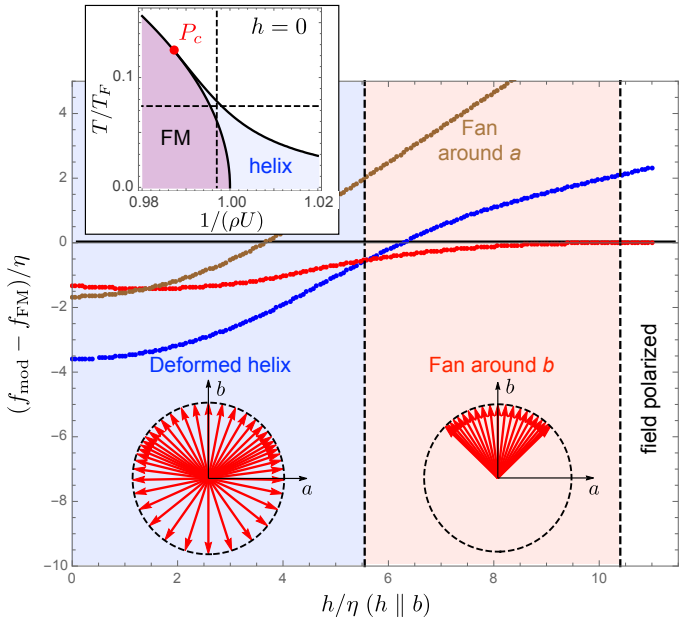

FIG. S3: Evolution of the free energies of the fan states and the deformed helix as a function of field along the hard in-plane direction evaluated for $1/(\rho U) = 0.997$ and $T/T_F = 0.074$ (these coordinates are shown as a cross hair in the inset phase diagram). The transition from the deformed helix to the field-polarized ferromagnet occurs through an intermediate fan state around the field direction.

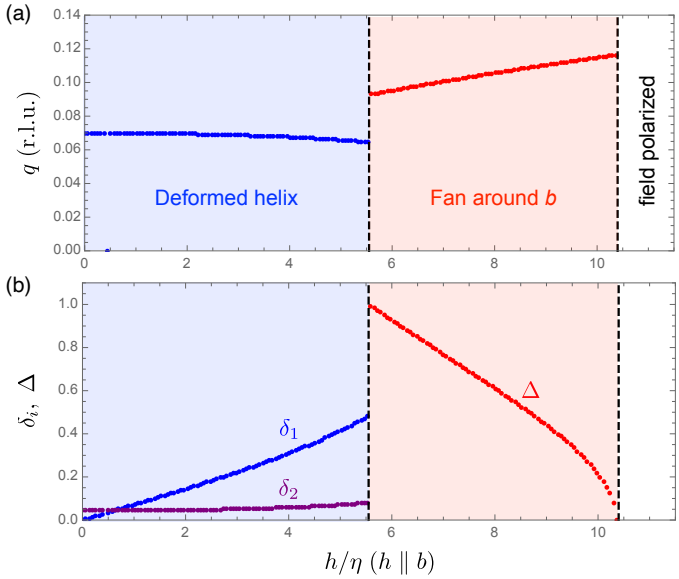

FIG. S4: Field dependence of (a) the ordering wavevector q and (b) the deformations δ_1, δ_2 of the helix and the opening angle Δ of the fan.

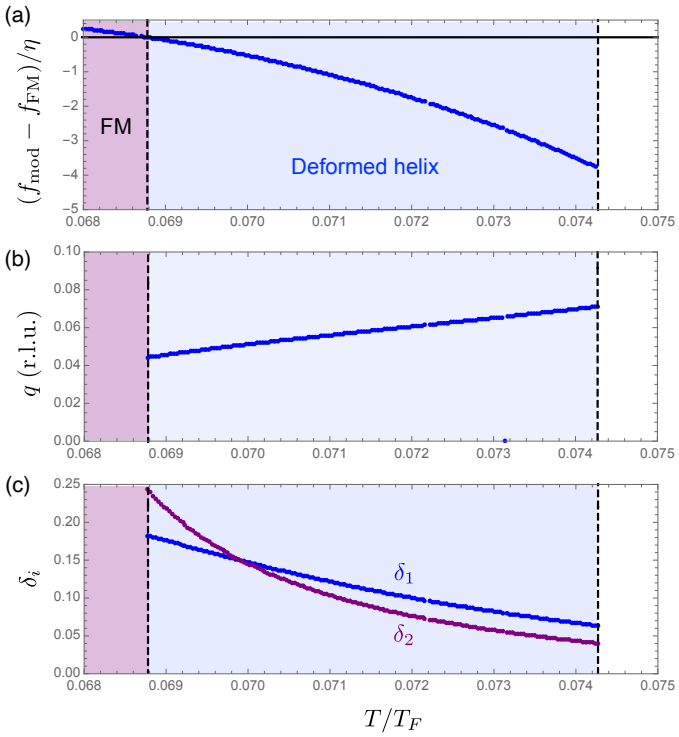

FIG. S5: Temperature dependence of (a) the free energy, (b) the ordering wavevector q and (c) the deformations δ_1 and δ_2 of the deformed helix state at fixed field.

[1] G. Abdul-Jabbar, D. A. Sokolov, C. D. O'Neill, C. Stock, D. Wermeille, F. Demmel, F. Krüger, A. G. Green, F. Lévy-Bertrand, B. Grenier, et al., Nat. Phys. **11**, 321 (2015).
[2] S. Kato, H. Kitazawa, H. Abe, N. Tsujii, and G. Kido, Physica B: Condensed Matter **294-295**, 217 (2001).
[3] D. Belitz, T. R. Kirkpatrick, and T. Vojta, Phys. Rev. Lett. **82**, 4707 (1999).
[4] A. V. Chubukov, C. Pépin, and J. Rech, Phys. Rev. Lett. **92**, 147003 (2004).
[5] J. A. Hertz, Phys. Rev. B **14**, 1165 (1976).
[6] A. J. Millis, Phys. Rev. B **48**, 7183 (1993).
[7] A. G. Green, G. Conduit, and F. Krüger, Annual Review of Condensed Matter Physics **9**, 59 (2018).
[8] U. Karahasanovic, F. Krüger, and A. G. Green, Phys. Rev. B **85**, 165111 (2012).
[9] C. J. Pedder, F. Krüger, and A. G. Green, Phys. Rev. B **88**, 165109 (2013).